JOURNAL OF AIRCRAFT
Vol. 36, No. 3, May–June 1999

Rigid and Flexible Low Reynolds Number Airfoils

Wei Shyy,* Fredrik Klevebring,† Mikael Nilsson,† Jason Sloan,† Bruce Carroll,‡ and Carlos Fuentes†
University of Florida, Gainesville, Florida 32611

Issues related to the design of low Reynolds number airfoils, such as the thickness, camber, and surface profiles, are investigated. To contrast the issues involved, NACA 0012 and CLARK-Y, two well-known airfoils, a recently proposed low Reynolds number airfoil S1223, and a modified airfoil UF, are compared under varied Reynolds numbers and angles of attack. These airfoils range from 0% (NACA 0012) to 8.89% (S1223) camber, and from 6% (UF) to 12.9% (CLARK-Y) thickness, and allow us to make a broad comparison of the lift-and-drag characteristics with varying Reynolds numbers, from 7.5×10^4 to 2.0×10^6. Furthermore, the concept of a flexible airfoil is assessed in an unsteady, low Reynolds number environment. To facilitate the present study, we have employed techniques treating either inviscid or coupled inviscid/boundary-layer flows around rigid airfoils, as well as a moving boundary technique to handle an elastic, massless membrane in a portion of the upper airfoil surface. The results show that within the range of Reynolds numbers and airfoil shapes, increased camber and reduced thickness provide more favorable lift-and-drag characteristics when the Reynolds number becomes lower. The results also indicate that a flexible profile yields better overall performance than a similar rigid profile in an oscillating freestream.

Nomenclature

C_d = drag coefficient
C_l = lift coefficient
C_p = pressure coefficient
c = airfoil chord
E = elastic modulus
h = membrane thickness
L = length of the membrane after deformation
L_0 = prestrained length of the membrane
P = flight power requirement
p = pressure
p_{in} = pressure on the inside of the airfoil
p_{out} = pressure on the outside surface of the airfoil
q_∞ = freestream stagnation pressure, $\frac{1}{2}\rho V_\infty^2$
Re = freestream Reynolds number, $V_\infty c/\nu$
S = wing planform area
$^\circ S$ = membrane prestress
s = surface coordinate
T = membrane tension
V_∞ = freestream velocity
W = weight of aircraft
α = angle of attack
δ = membrane strain
θ_i = surface slope angle
θ_∞ = momentum thickness of the wake at downstream infinity
κ = membrane curvature
Π_1 = membrane equilibrium parameter, $(Eh/q_\infty c)$
ρ = density

Introduction

THERE has recently been a growing interest in designing micro-sized aircraft for a variety of military and civilian applications. Such aircraft have come to be known as micro air vehicles (μAVs) and are currently characterized by length scales under 15 cm and flight speeds of ~15 m/s. μAVs are being designed to conduct specific tasks that may be dangerous or inaccessible to humans. The initial applications for μAVs will likely be for the military, where they will conduct missions that involve local reconnaissance and communication. This technology could also be useful in civilian applications such as survivor search-and-rescue, chemical-spill monitoring, and agricultural development, where onboard instruments can retrieve visual, chemical, and biological information. Designing a μAV is a highly multidisciplinary task; competing designs will require innovation in aerodynamics, controls, propulsion, and instrumentation. The rapid progress made in the area of miniaturization of sensors, actuators, and communication devices has made μAVs feasible; however, reduced physical dimensions and slow flight speeds also means deteriorating aerodynamic performance of the flight vehicles.

An airfoil's performance may be expressed in terms of its lift-to-drag ratio C_l/C_d, or perhaps more accurately in terms of the flight power requirement P, given by[1–3]

$$P = W\left(C_d \Big/ C_l^{\frac{3}{2}}\right)\sqrt{(2/\rho)(W/S)} \tag{1}$$

The coefficients for a given profile are functions of both the angle of attack and the freestream Reynolds number. In the low-speed flight environment of μAVs, the variation in wind velocity is substantial compared with the flight velocity, causing the angle of attack and Reynolds number to fluctuate considerably.[4] The effect of this unsteadiness on aircraft performance is readily observed at radio-controlled airplane competitions, where sudden, uncontrolled aircraft motions frequently result in crashes. μAVs require airfoils capable of sustaining good performance over a range of flow conditions.

The Reynolds numbers of currently envisioned μAVs lie in the range 10^4–10^5. At such low Reynolds numbers, the flow surrounding the leading-edge region is usually laminar. Consequently, the boundary-layer fluid momentum is often not strong enough to overcome the adverse pressure gradient on the aft-side of the airfoil, and laminar separation occurs.[5] The extent of the separation bubble is dependent on the Reynolds number. Furthermore, the location and structure of separated regions are very sensitive to small changes in flow conditions, making it difficult to construct optimized or even working airfoils for the fluctuating environment of μAVs. An interesting alternative that would improve the aerodynamics of a wing would be to change the shape of the wing during flight. An adaptable wing could have noticeable effects on sustaining good performance in a fluctuating environment.[6] With intelligently designed sensing

Received April 6, 1998; revision received Nov. 4, 1998; accepted for publication Nov. 17, 1998.

*Professor and Chairman, Department of Aerospace Engineering, Mechanics and Engineering Science. Associate Fellow AIAA.
†Graduate Student, Department of Aerospace Engineering, Mechanics and Engineering Science.
‡Associate Professor, Department of Aerospace Engineering, Mechanics and Engineering Science. Member AIAA.

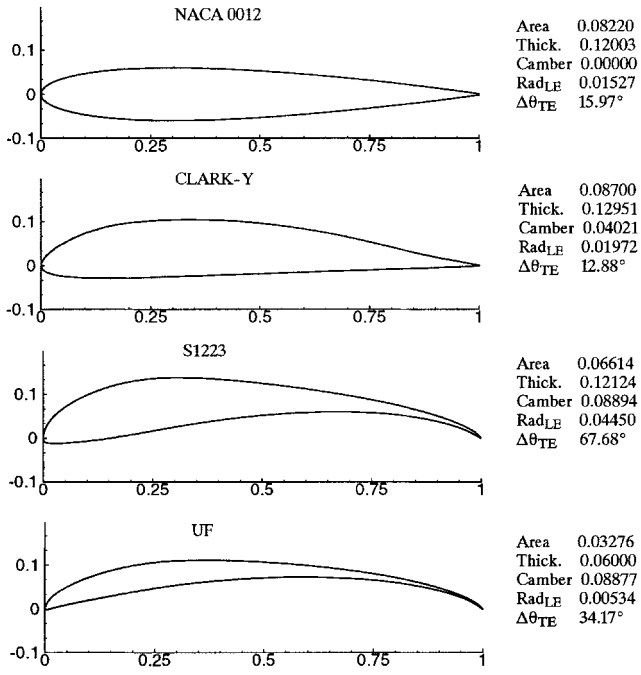

Fig. 1 Four airfoils chosen for initial assessment.

and control strategies, changes in freestream conditions can be detected, and actuators can be placed to dynamically adjust the camber and shape of the wing. At higher angles of attack, much of the wing may be masked by the separation bubble, and a larger displacement of the wing surface and/or camber would be necessary. An integrated approach to simultaneously account for aerodynamics and sensing/control considerations will be highly desirable. A combination of passive and active control strategies offers an opportunity for improving μAV aerodynamics. To reduce the tendency of flow separation in this manner, a flexible adaptive wing seems attractive. However, before such an adaptive concept can be successful, it is important to thoroughly explore the interplay between the airfoil characteristics, such as camber and thickness, and the flow environment, such as the Reynolds number and angle of attack, so that appropriate guidance can be devised.

In the present study, we investigate these issues directly related to low Reynolds number aerodynamics. We have selected two well-known airfoils, NACA 0012 and CLARK-Y, a recently proposed low Reynolds number airfoil, S1223,[7] and one modified airfoil based on S1223, which we call UF. UF has a camber profile very close to S1223, but has a smaller thickness, 6% vs S1223's 12.124% chord. Figure 1 shows the profiles of the four airfoils. Next, the concept of a flexible airfoil is assessed in an unsteady, low Reynolds number environment. To facilitate the present study, we have employed techniques treating either inviscid or coupled inviscid/boundary-layer flows around rigid airfoils, as well as a moving boundary technique to handle an elastic, massless membrane in a portion of the upper airfoil surface. The results show that within the range of Reynolds numbers and airfoil shapes, increased camber and reduced thickness provide more favorable lift and drag characteristics when the Reynolds number becomes lower.

Computational Methodology and Software

Airfoil design procedures require a fast and robust analysis method for performance evaluation. For a given cost and time schedule, a fast analysis permits faster optimization than a slower method of comparable accuracy, and thus, allows more time to be spent on detailed analysis using, e.g., a Navier–Stokes solver. For low Reynolds number airfoils considered in the present work ($Re = 10^4$–10^5), the demands on the analysis method become even more severe. Accurate representation of both laminar and turbulent separated flow is a must because transitional separation bubbles and their losses must be accurately calculated if accurate drag predictions are to be obtained. The transition prediction algorithm must also be reliable because it effects the termination point of any transitional separation bubble, and, hence, determines the bubble's size and associated losses. To facilitate the present study, we have employed XFOIL,[8] which models inviscid or coupled inviscid/boundary-layer flows around rigid airfoils in steady, subsonic flow.

XFOIL uses a two-equation boundary-layer integral formulation based on dissipation closure for both laminar and turbulent flows.[9] In the laminar formulation XFOIL includes a transition prediction formulation based on spatial amplification theory. In the turbulent formulation XFOIL also includes a lag equation to account for lags in the response of the turbulent stresses to changing flow conditions. The inviscid freestream is computed using a linear-vorticity panel method. The boundary-layer and transition equations are solved simultaneously with the inviscid flowfield by a global Newton method.

The airfoil contour and wake trajectory are discretized into flat panels. A linear vorticity distribution is associated with each airfoil panel. Each airfoil and wake panel also have a constant source strength that are related to viscous layer quantities. The viscous formulation employs the integral momentum and kinetic energy shape parameter equations, and a shear-stress lag equation is used in the turbulent flow region. For the laminar regions, a rate equation is adopted to model the growth of the amplitude of the most amplified Tollmien–Schlichting wave. The drag coefficient C_d is obtained from the Squire–Young formula, namely,

$$C_D = 2\theta_\infty / c \tag{2}$$

where the momentum thickness of the wake at downstream infinity θ_∞ is obtained by extrapolation of the momentum thickness from the last panel of the wake. More details can be found in Refs. 8 and 9.

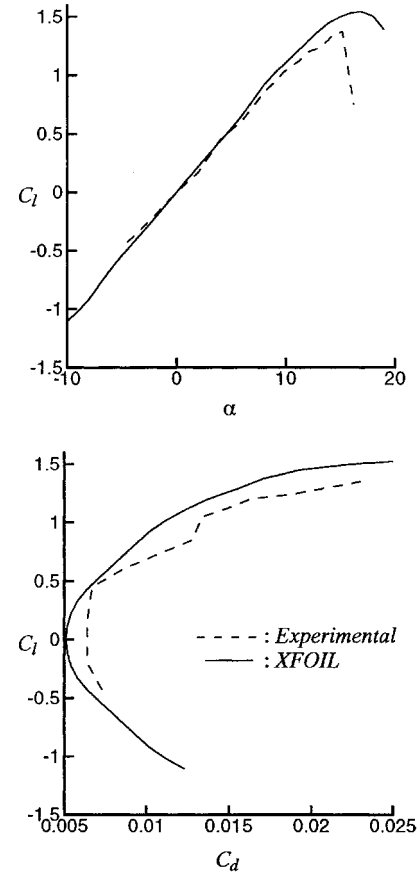

Fig. 2 Comparison of experimental and predicted aerodynamic performance of the NACA 0012 profile at $Re = 2.0 \times 10^6$.

Aerodynamic Assessment of Four Rigid Airfoils

We will first examine XFOIL based on a comparison with available experimental data to assess its predictive capability. The four airfoils were chosen because they cover different shape characteristics, ranging from 0% (NACA 0012) to 8.89% (S1223) camber, and from 6% (UF) to 12.9% (CLARK-Y) thickness. Together, these airfoils allow us to make a broad comparison of the lift-and-drag characteristics with varying Reynolds numbers, from 7.5×10^4 to 2.0×10^6.

Figure 2 depicts the aerodynamic performance, in the form of lift coefficient vs angle of attack and the lift-to-drag polar plot, of the NACA 0012 profile at $Re = 2.0 \times 10^6$, a high Reynolds number at which experimental measurements are readily available. The computations are conducted based on the coupled viscous–inviscid flow solutions by changing the input angle of attack. For the C_l vs α plot, the agreement is satisfactory in terms of the lift coefficient before stall as well as the α at which the airfoil stalls. The predicted $C_l - C_d$ polar plot also largely follows the experimental measurement, albeit with discrepancies at certain points. Experimental data for the NACA 0012 profile were taken from Ladson.[10] For the CLARK-Y airfoil, a series of measurements were performed at the University of Florida. Figure 3 shows C_p plots for incident angles from 0 to 10 deg at a Reynolds number around 2.0×10^5 for the CLARK-Y profile. Both inviscid and coupled viscous–inviscid flow models are employed to help assess the performance of the code. For α ranging between 0 and 4 deg, the inviscid and the viscous–inviscid models yield results closely resembling each other, except at the predicted bubble locations. As the angle of attack increases beyond 6 deg, the viscous–inviscid model produces results in noticeably better agreement with the experimental measurements.

For the S1223, experiments are performed in a Reynolds number span between 1.0×10^5 and 3.0×10^5 by Selig and Guglielmo.[7] Figure 4 shows that the viscous–inviscid model seems to overpredict the C_l/C_d in general, and the discrepancies between predictions and measurements widen as the Reynolds number becomes lower. Nevertheless, both the theory and the experiment confirm that the aerodynamic performance degrades as the Reynolds number is reduced. Combining Figs. 2–4, we conclude that overall, the XFOIL code does a better job for higher Reynolds number flows; its predictability becomes worse as the Reynolds number decreases. However, there is insufficient information to assess the accuracy of the experimental data of S1223. Nevertheless, it seems that, as expected, XFOIL is adequate to be used as a tool to discern the relative aerodynamic performance between different airfoils.

A systematic effort is made to examine the relative performance of the four airfoils with different Reynolds numbers. First, a number of calculations are made to investigate aerodynamic characteristics of the four airfoils shown in Fig. 1. Figures 5 and 6 show the $C_l^{3/2}/C_d$ and C_l/C_d plots. Several observations can be readily made:

1) For all airfoils, the C_l/C_d ratio exhibits a clear Reynolds number dependency. Between Re of 7.5×10^4 and 2.0×10^6, C_l/C_d changes by a factor of 2–3 for all airfoils tested.

2) Except for the UF airfoil, which is very thin, the range of angle of attack within which aerodynamics is satisfactory becomes narrower as the Reynolds number decreases.

3) Clearly, the camber is important. NACA 0012, with 0% camber, and CLARK-Y with 3.5% camber, yield less satisfactory performance in all three Reynolds numbers. S1223 and UF, both with 8.89% camber, perform better.

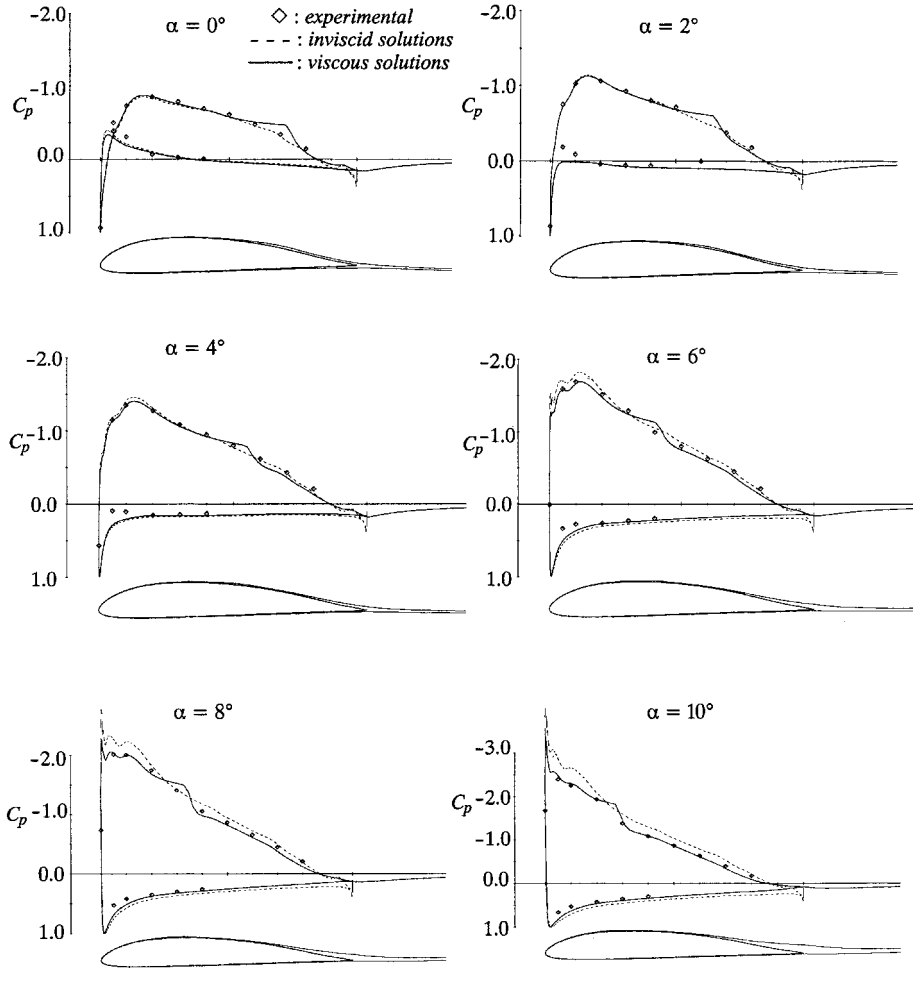

Fig. 3 Comparison of predicted and measured C_p plots for the CLARK-Y profile at $Re = 2 \times 10^5$ and different angles of attack.

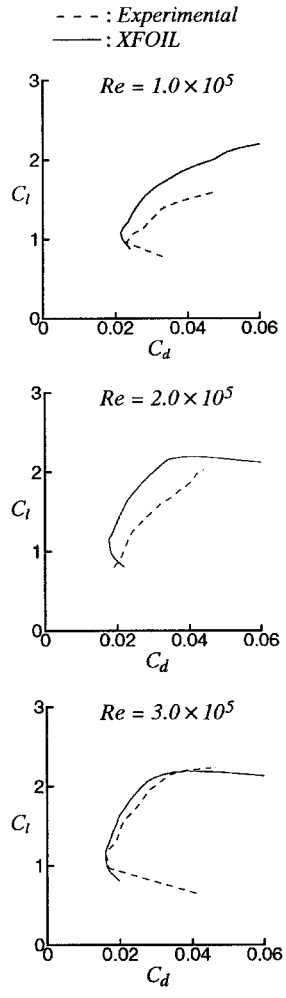

Fig. 4 Comparison of experimental and predicted polar plots for the S1223 profile.

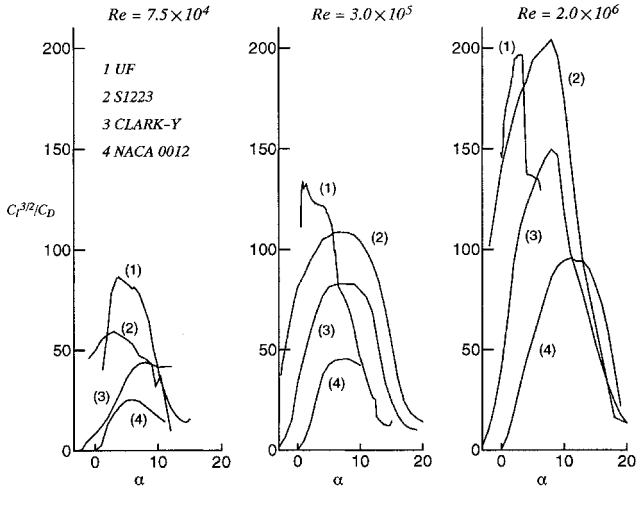

Fig. 5 $C_l^{3/2}/C_d$ plots at three different Reynolds numbers.

4) NACA 0012, CLARK-Y, and S1223 all have a maximum thickness of $\sim 0.12c$. The UF airfoil, on the other hand, is much thinner, with a maximum thickness of $0.06c$. It is interesting to compare the results between $Re = 7.5 \times 10^4$ and 2.0×10^6. At $Re = 2.0 \times 10^6$, S1223 and UF have comparable peak performance in terms of $C_l^{3/2}/C_d$ and C_l/C_d; however, S1223 exhibits a wider range of acceptable angles of attack. At $Re = 7.5 \times 10^4$, the situation is quite different. UF, the thinner airfoil with identical camber, exhibits substantially better aerodynamic performance while maintaining a range of acceptable angles of attack comparable to that of S1223.

One should note that to judge the power requirement based on Eq. (1), one must consider the aerodynamic parameters of the entire aircraft. Because our interest in the present study is to ascertain the relationship between airfoil shapes and the Reynolds number, we don't have adequate information to examine the information related to the induced drag and other components such as fuselage. However, in the context of μAVs, power consumption is a most critical issue because of the degraded aerodynamic performance of the wing. Accordingly, in Figs. 5 and 6, we choose to show both $C_l^{3/2}/C_d$ and C_l/C_d vs the angle of attack at different Reynolds number to emphasize our interest in addressing this concern. Together, one can deduce from Figs. 5 and 6 any information related to C_l and C_d in other forms such as polar plots.

Flexible Airfoil

Many flying machines from self-inflating parawings to birds are using lifting surfaces that significantly deform. With the right choice of materials, pretension, and unstrained shape, an aerodynamically effective equilibrium configuration can often be achieved to improve the flight performance. This has historically been an intuitive and empirical art of sail makers and wing designers. However, computational methods have begun to emerge to simulate flight-involving membranes, as documented in Refs. 11–13. To gain further knowledge of the benefits involved with adaptive profiles, XFOIL was modified to handle airfoils with membrane surfaces and an unsteady freestream. To simulate airfoils with membrane surfaces, the equations of membrane equilibrium must be incorporated into the overall solution. A portion of the top surface (from $0.1c$ to $1.0c$) is assumed to be a massless membrane that will instantaneously adjust its shape according to the membrane equilibrium equation:

$$\kappa = -\left(1/\Pi_1^3\right)(\Delta p/T) \tag{3}$$

Because the membrane is considered to be massless, Eq. (3) is valid in both steady and unsteady flow environments. The tension T is given by

$$T = (^{\circ}S + E\delta)h \tag{4}$$

where δ is given by

$$\delta = (L - L_0)/L_0 \tag{5}$$

As discussed in Shyy et al.,[11] for situations when the membrane tension is dominated by elastic strain, Π_1 is given by

$$\Pi_1 = (Eh/q_\infty c)^{\frac{1}{3}} \tag{6}$$

Based on the dimensional inspection, the value of Π_1 is related to the time scale ratio between the fluid and the membrane to the $\frac{3}{2}$ power. The pressure difference is defined as the difference between the outside and the inside of the airfoil, which is set equal to the stagnation pressure:

$$\Delta p = p_{\text{out}} - p_{\text{in}} = q_\infty (C_p - 1) \tag{7}$$

The surface slope angles θ_i and θ_{i+1}, shown in Fig. 7, are determined from the curvature as[14]

$$\frac{d\theta}{ds} = \kappa \tag{8}$$

which upon integrating is

$$\theta_{i+1} = \theta_i + \kappa \Delta s \tag{9}$$

Assuming κ to be constant between two adjacent points and taking an initial guess for θ_1, the new membrane coordinates can be successively calculated using the angles and curvatures shown in Fig. 7. The last point on the membrane most likely will not match the trailing edge of the bottom surface where the membrane is supposed to attach. The shooting method is used to iterate the membrane shape

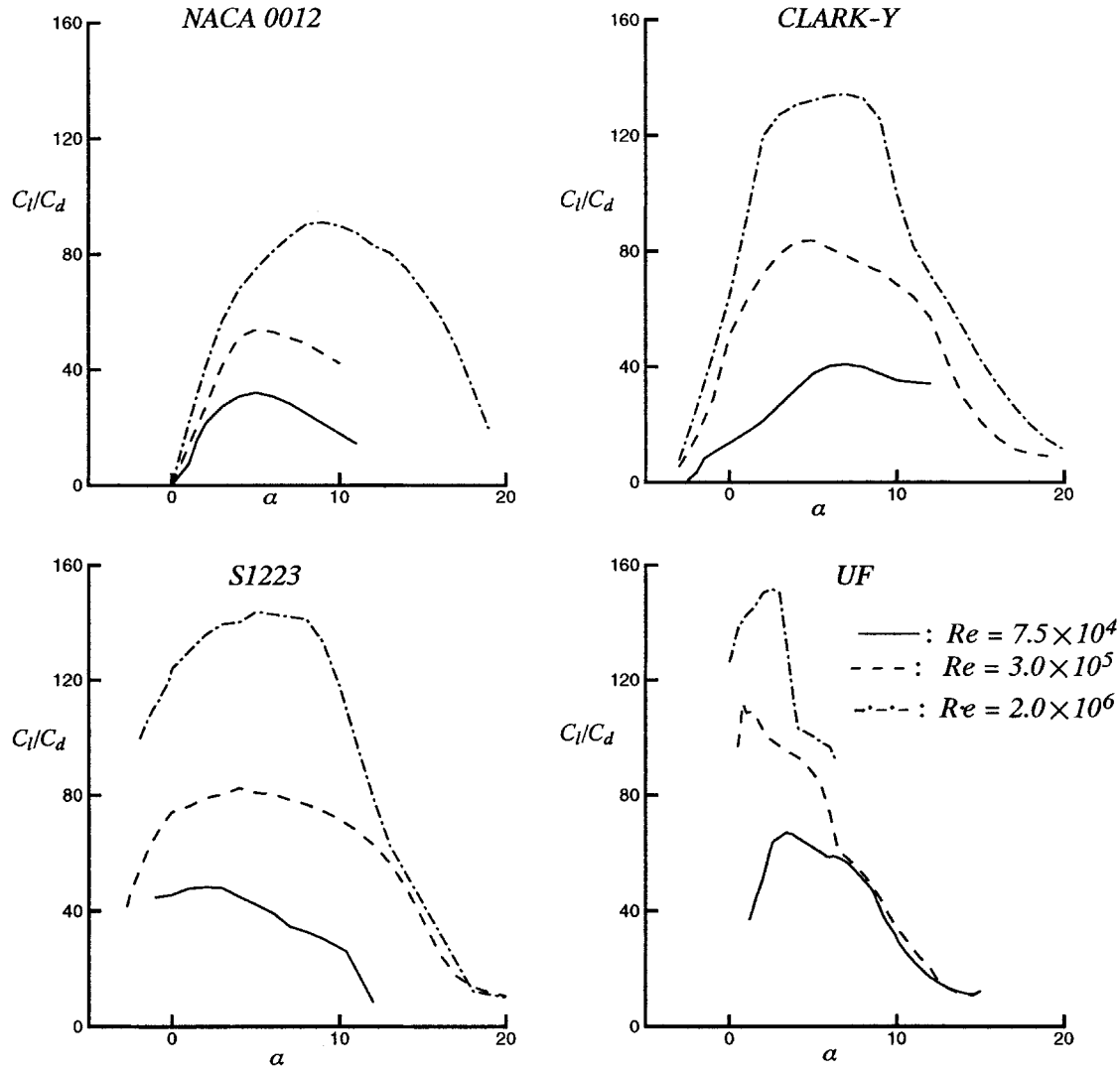

Fig. 6 C_l/C_d vs α plots for the four airfoils.

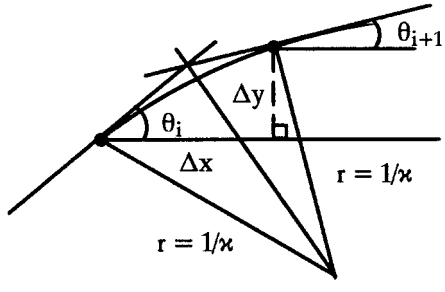

Fig. 7 Membrane coordinate calculation.

by altering the initial guess angle θ_1. The procedure converges when the membrane's trailing-edge y coordinate coincides with the rigid trailing-edge y coordinate of the bottom surface (a small correction for the x coordinate is then made). A new pressure distribution is then calculated, and another membrane shape is determined corresponding to the new pressure difference. An equilibrium shape is reached when the coordinate changes in two successive profiles are smaller than a certain value ε. The freestream velocity is time-stepped in a sinusoidal pattern, and the entire procedure is repeated to obtain a new equilibrium shape corresponding to the new boundary conditions.

Having extended XFOIL to simulate oscillating flow around two-dimensional membrane-top airfoil profiles, a number of computations are done to establish the possible benefits of this configuration.

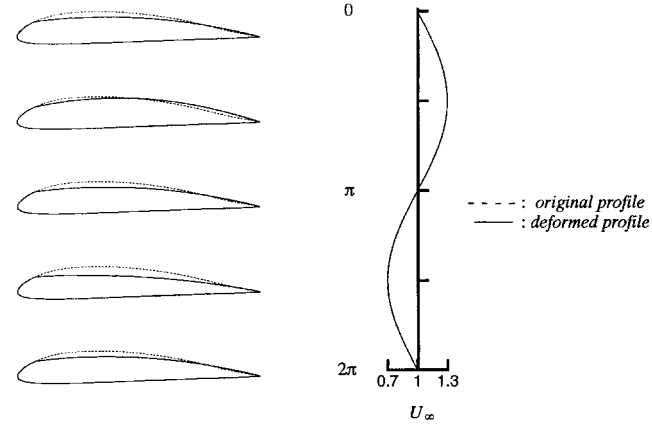

Fig. 8 Membrane deformations during a full-period oscillation of the freestream velocity with $Re_{mean} = 8.0 \times 10^4$.

A CLARK-Y profile served as the base shape, upon which a membrane top was attached. Computations for a Reynolds number oscillating around 8.0×10^4 were made for both a rigid and a flexible case to compare the influence of the membrane. An example of the movements of the membrane top for a CLARK-Y profile during a full-period oscillation of the freestream velocity for $Re = 8.0 \times 10^4$ with $\Pi_1 = 8.8$ (indicating that the time-scale ratio between the fluid and the membrane is about 26) and $\delta = 0$ is displayed in Fig. 8. The

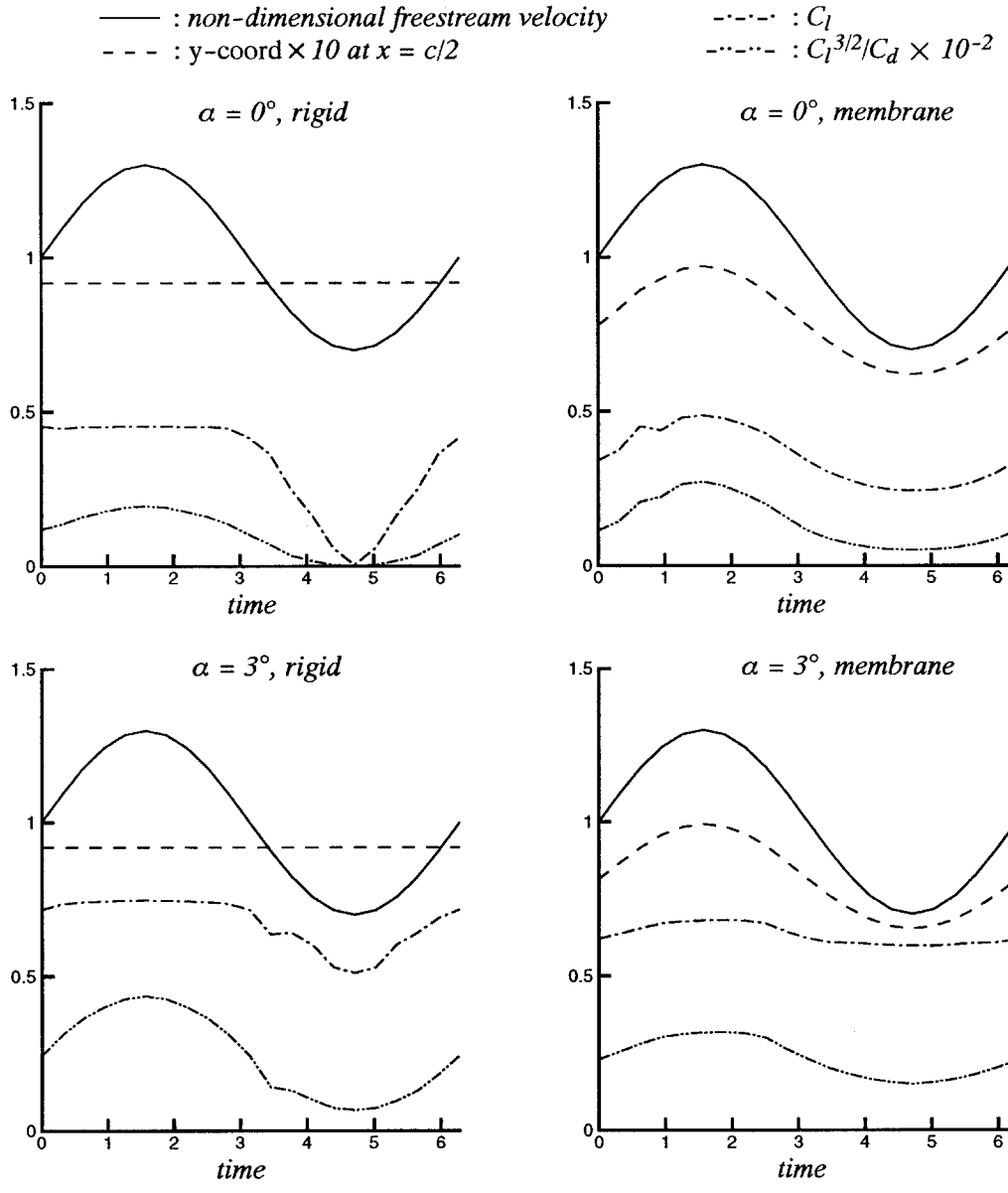

Fig. 9 Comparison between rigid and membrane CLARK-Y profile at $Re = 8.0 \times 10^4$.

time-series plots are based on dimensional quantities. In physical terms, the freestream velocity, also shown in time-series plots, has a mean value of 10 m/s and fluctuates by ±30% about the mean. The frequency of the freestream oscillation is 1 Hz, giving a Strouhal number of 0.10. The time-dependent lift coefficient and power index is displayed in Fig. 9.

For both $\alpha = 0$ and 3 deg, the lift coefficient of the rigid profile breaks down as the freestream velocity approaches and reaches a minimum. The maximum lift coefficients of the flexible airfoil are no better than those of the rigid airfoil; however, the flexible airfoil exhibits less sensitivities to oscillations in the freestream, and yields overall more favorable aerodynamic characteristics. The wide performance gap can best be seen for the zero angle-of-attack case in Fig. 9. Qualitatively, the membrance curvature adjusts in accordance with the flight speed. This behavior shows that the flexible airfoils is adaptive in shape, in response to the instantaneous flow physics around the airfoil. The instantaneous airfoil shape is consistent with the previous observation under the steady-state flow condition that a thinner airfoil performs better with a reduced Reynolds number. Similar conclusions have been drawn in work by Shyy and Smith,[6] where a thin membrane airfoil was compared with a similar rigid airfoil.

Conclusions

To assess aerodynamic performance in the Reynolds number range of interest, S1223 shows good flight performance compared with NACA 0012 and CLARK-Y, thus implying that a higher camber airfoil is preferable. Within the range of the Reynolds number considered, the modified airfoil, UF, shows improved aerodynamic characteristics over the S1223 with decreasing Reynolds number, thus implying the benefits of reduced thickness. XFOIL was modified to simulate membrane-top airfoils in an attempt to identify robust airfoils for the unsteady flow environment of μAVs. When compared with the corresponding rigid profile in a low Reynolds number, oscillating freestream, the flexible upper surface provides a more stable lift coefficient and $C_l^{3/2}/C_d$ performance. These results are similar to those previously obtained by Shyy and Smith[6] for a zero-thickness membrane. It appears that μAV wings can be designed with the attributes identified in this study to provide improved performance.

Acknowledgments

This work was partially supported by the U.S. Air Force Office of Scientific Research and The Boeing Company.

References

[1]Anderson, J. D., Jr., *Introduction to Flight*, 3rd ed., McGraw–Hill, New York, 1989.

[2]Donovan, J. F., and Selig, M. S., "Low Reynolds Number Airfoil Design and Wind Tunnel Testing at Princeton University," *Low Reynolds Number Aerodynamics*, Springer–Verlag, New York, 1989, pp. 39–57.

[3]Foch, R. J., and Ailinger, K. G., "Low Reynolds Number, Long Endurance Aircraft Design," AIAA Paper 92-1263, 1992.

[4]Liu, H.-T., "Unsteady Aerodynamics of a Wortmann Wing at Low Reynolds Numbers," *Journal of Aircraft*, Vol. 29, No. 4, 1992, pp. 532–539.

[5]Mueller, T. J. (ed.), *Low Reynolds Number Aerodynamics*, Springer–Verlag, New York, 1989.

[6]Shyy, W., and Smith, R., "A Study of Flexible Airfoil Aerodynamics with Application to Micro Aerial Vehicles," AIAA Paper 97-1933, July 1997.

[7]Selig, M. S., and Guglielmo, J. J., "High-Lift Low Reynolds Number Airfoil Design," *Journal of Aircraft*, Vol. 34, No. 1, 1997, pp. 72–78.

[8]Drela, M., "XFOIL: An Analysis and Design System for Low Reynolds Number Airfoils," *Low Reynolds Number Aerodynamics*, Springer–Verlag, New York, 1989, pp. 1–12.

[9]Drela, M., and Giles, M. B., "Viscous-Inviscid Analysis of Transonic and Low Reynolds Number Airfoils," *AIAA Journal*, Vol. 25, 1987, pp. 1347–1355.

[10]Ladson, C. L., "Effects of Independent Variation of Mach and Reynolds Numbers on the Low-Speed Aerodynamic Characteristics of the NACA 0012 Airfoil Section," NASA TM-4074, 1988.

[11]Shyy, W., Udaykumar, H. S., Rao, M. M., and Smith, R., *Computational Fluid Dynamics with Moving Boundaries*, Taylor and Francis, Washington, DC, 1996.

[12]Smith, R. W., and Shyy, W., "Incremental Potential Flow Based Membrane Wing Element," *AIAA Journal*, Vol. 35, No. 5, 1997, pp. 782–788.

[13]Smith, R. W., and Shyy, W., "Computation of Aerodynamic Coefficients for a Flexible Membrane Airfoil in Turbulent Flow," *Physics of Fluids*, Vol. 8, No. 12, 1996, pp. 3346–3353.

[14]Kessler, D. A., Koplik, J., and Levine, H., "Pattern Selection in Fingered Growth Phenomena," *Advances in Physics*, Vol. 37, No. 2, 1988, pp. 255–339.